JOURNAL OF MATERIALS SCIENCE 21 (1986) 511–521

Surface features and plasticity induced by tension–tension fatigue of Inconel 718

R. P. KHATRI, R. N. PANGBORN
Department of Engineering Science and Mechanics, The Pennsylvania State University, University Park, Pennsylvania 16802, USA

T. S. COOK, M. ROBERTS
Aircraft Engine Group, Materials Life and Methods, General Electric Company, 1 Neumann Way, Cincinnati, Ohio 45215, USA

The accumulation of fatigue damage in Inconel 718 has been investigated with a combination of X-ray diffraction techniques and scanning electron microscopy. X-ray line broadening analyses and computer-aided rocking curve measurements have been conducted for solution-treated and age-hardened specimens, cycled in tension–tension. The line profile breadths were found to be very sensitive to the magnitude of the constant stress amplitude employed in the fatigue testing. After increasing sharply during the initial 15% of the fatigue life to a value which depends on the maximum stress level, the breadths are relatively invariant during the remainder of the life. The rocking curve breadths obtained using double crystal diffractometry, on the other hand, increase progressively with continued cycling from about 20% of the life to failure and are nearly independent of the stress amplitude used in the fatigue testing. These techniques can be applied effectively in combination to determine prior cyclic history by providing information on both the stress level and expended fraction of life. Therefore, application of the X-ray diffraction analyses to spectrum fatigue tests has been initiated, beginning with sequences involving regular decrements in the stress level. In order to evaluate differences in the response of the surface layer and the bulk material during fatigue, depth studies have also been carried out. The development of topographical features, such as slip bands, and their relationship to crack initiation and propagation mechanisms have been examined by scanning electron microscopy and correlated to the X-ray diffraction data.

1. Introduction

Owing to its extensive use in gas turbines, Inconel 718 must withstand cyclic deformation at temperatures up to 900 K. Numerous investigations have been conducted on the low cycle fatigue behaviour of this alloy [1–6]. In most investigations of alloy 718, the fatigue tests were performed under strain control and the specimens were prepared from age-hardened material. This paper, however, deals with load-controlled fatigue tests performed on both solution-treated and age-hardened material. Load-controlled fatigue behaviour and properties for both material conditions have been established and are compared to the low cycle, strain-controlled test results.

The physical metallurgy of this alloy has been studied by Kirman and Warrington [7]. Instead of aluminium or titanium, niobium is the hardening addition. So, unlike most of the other nickel-base alloys, the major hardening precipitate in alloy 718 is a Ni_3Nb phase.

A number of X-ray diffraction methods have been developed which are useful in evaluating the stress and strain states of deformed crystalline materials. These include X-ray residual stress analysis, X-ray line broadening analysis, and X-ray rocking curve measurements made using a double crystal diffractometer. All of these methods can be applied non-destructively and are very sensitive to induced lattice deformations. The latter two techniques provide a sensitive measure of crystallographic distortions accrued during fatigue, as manifested by broadening of the line profiles or rocking curves, respectively.

X-ray line broadening measurements have been reported for numerous investigations attempting to correlate the changes in breadth to the expended fatigue life [8–16]. For the most part, the usefulness of the technique has been shown to reside in the correlation of line breadths to the stress level employed. The *average* plasticity, whether microscopic or macroscopic, incurred during the cycling influences the level of broadening measured for a particular cyclic stress level.

X-ray rocking curve analysis, as modified for application to polycrystalline metals, affords the capability to evaluate the distortion in individual grains of the specimen [17–22]. Rather than reflecting simply the average level of plasticity, this technique is better suited to examine the local deformations and to isolate those grains undergoing large distortions (as a result of favourable orientation for high resolved shear stress or due to proximity to stress concentrations)

0022–2461/86 $03.00 + .12

from those which are relatively unaffected by the fatigue cycling.

In this investigation, both line profile breadths and rocking curve breadths were monitored during the life for specimens cycled to failure at various constant stress amplitues. Subsequently, the effect of decreasing the maximum stress *during* the fatigue life on the rocking curve and the line profile breadths was investigated. The objective of the spectrum fatigue study was to evaluate whether expended life could be determined with no prior knowledge of cyclic history.

The surface morphology of the specimens was studied and correlated to the X-ray diffraction data in order to identify the mechanisms of deformation and failure. Scanning electron micrographs were taken at progressively higher fractions of life for specimens tested at each stress level.

2. Experimental procedure

2.1. Material and testing

Cylindrical specimens of gauge diameter 3.17 mm and gauge length of 10 mm were machined from solutionized alloy 718. After machining, the surfaces were ground with successively finer grits and electropolished (85% glacial acetic acid, 15% perchloric acid; 12 V, 0.1 A; 10 to 15° C; with agitation) to remove about 35 μm from the surface. Residual damage and stresses due to machining and grinding operations were considered absent after this surface preparation as shown by the invariance of line profile and rocking curve breadths from the surface into the bulk. The specimens were axially fatigued in tension–tension with $R = 0.1$ and the maximum stress was varied from 1.10 to 1.75 times the yield strength. All fatigue tests were conducted at a frequency of 25 Hz.

The second phase of study was conducted using age-hardened material. Heat treatment was performed as specified in ASTM B637-84 [23], omitting the second ageing step: the material was solutionized at 960° C for 1 h, followed by a water quench; aged at 718° C for 8 h and air cooled. Despite constant flushing with argon, a thin oxide layer formed which was removed by lapping with alumina and subsequent electropolishing. The maximum stress employed in the fatigue testing of aged specimens was varied from 0.6 to 1.1 times the yield strength.

2.2. X-ray diffraction

X-ray line broadening analysis was carried out using a GE XRD-5 diffractometer modified for step scanning and coupled to an Apple-II plus microcomputer. X-ray counts were collected for 20 sec in steps of 0.005° through the diffraction peak. The line profile breadths were determined from the peak profile after smoothing, background removal and Rachinger correction [24] were performed.

In double crystal diffractometry (DCD), a highly parallel, crystal-monochromated X-ray beam is made to impinge on the specimen. Incremental rotation of the specimen causes the randomly oriented grains to pass through angles corresponding to their respective Bragg reflection conditions. The range over which each grain reflects a measurable X-ray count is recorded as a function of the angle of specimen rotation. A rocking curve is thus obtained for each grain. In this investigation, a position sensitive detector coupled with a multichannel analyser and a VAX 11-730 computer were used to automate the analysis. The computer also controlled the stepping motor drive system employed to rotate the specimen. From the data, both the rocking curve halfwidth (full width at half maximum intensity) and the integral breadth (integrated intensity divided by the maximum intensity) could be computed for the rocking curve of each individual grain. Fig. 1 provides a schematic representation of the instrumentation.

3. Results and discussion

3.1. *S–N* diagrams

The tensile properties obtained for the specimen conditions investigated are as follows

$$\text{solution-treated: } \sigma_y\ (0.2\%) = 445\,\text{MPa},\quad \sigma_u = 864\,\text{MPa}$$

$$\text{aged: } \sigma_y\ (0.02\%) = 834\,\text{MPa},\quad \sigma_u = 1165\,\text{MPa}$$

These yield, σ_y, and ultimate strengths, σ_u, were compared to previous results and a close agreement was observed [25]. *S–N* diagrams for solution-treated and aged specimens have been established and are shown in Fig. 2. The data indicate that for both types of specimens, two distinct regimes exist, with a transition from high stress amplitude to low stress amplitude behaviour occurring at about two-thirds of the respective ultimate strength and 5×10^5 cycles. Similar behaviour has been reported by Tien and Gamble for Mar-M200 [26].

3.2. Scanning electron microscopy

Scanning electron micrographs were taken at various fractions of life for solution-treated specimens. Progressive cycling causes slip line formation and associated surface rumpling, as shown in Fig. 3. The stress axis is vertical for all scanning electron micrographs shown. The slip lines become denser on further cycling and intense deformation bands are formed. The fraction of life at which slip lines can just be distinguished, as well as first appearance of small fatigue cracks, depend on the maximum stress employed in the testing. Fig. 3 shows the comparable slip line development for specimens cycled to 5% of life at 779 MPa, 55% of life at 669 MPa and 81% of life at 559 MPa.

Initially the deformation is relatively homogeneous, but with continued cycling it becomes inhomogeneous and is concentrated in deformation bands. Cracks are initiated in these deformation bands and propagate along the bands, as shown in Fig. 4 and 5. Similar observations were made by Fournier and Pineau [5] in alloy 718 and Gell and Leverant [27] in Mar-M200. Fig. 4 also reveals that small fatigue cracks appear when specimen is cycled to 22% of life at 779 MPa and to 74% of life at 669 MPa. Fig. 5 illustrates that the direction of crack propagation is perpendicular to the stress axis macroscopically, but takes a path coinciding with either the slip bands or grain boundaries on a more local, or microscopic, level.

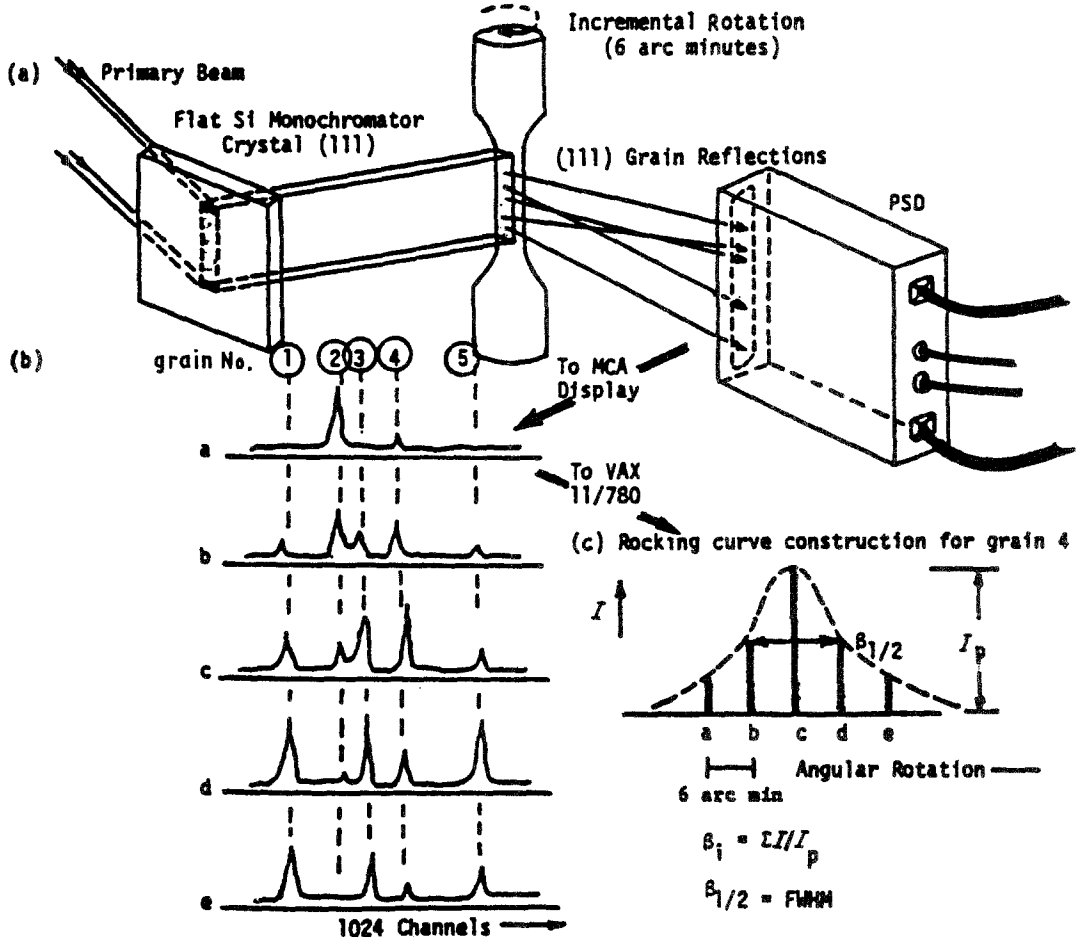

Figure 1 Schematic illustration of double crystal diffractometer. Reflections from individual grains are intercepted by position sensitive detector (a) and intensities of reflections are displayed by multi-channel analyser as separate peaks (b). Incremental specimen rotation allows evaluation of the reflecting range of each grain. Successive MCA displays a–e represent sample rotation intervals of 6 arc minutes (b). Data for each rotation position are stored and later used to construct the rocking curve for each grain. Reflection intensities for grain 4 at successive rotation positions a–e are shown horizontally in (c). Envelope of these represents the rocking curve for the grain. Halfwidths and integrated breadths are determined for all reflecting grains.

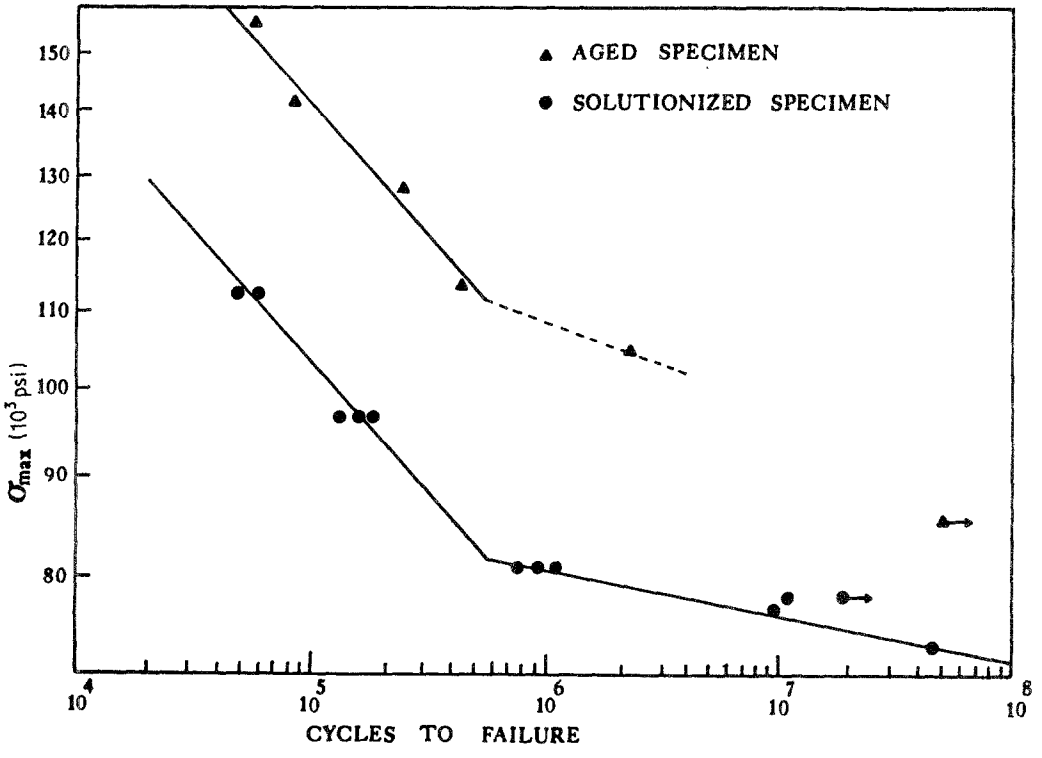

Figure 2 *S–N* diagrams for solution-treated and aged conditions of alloy 718.

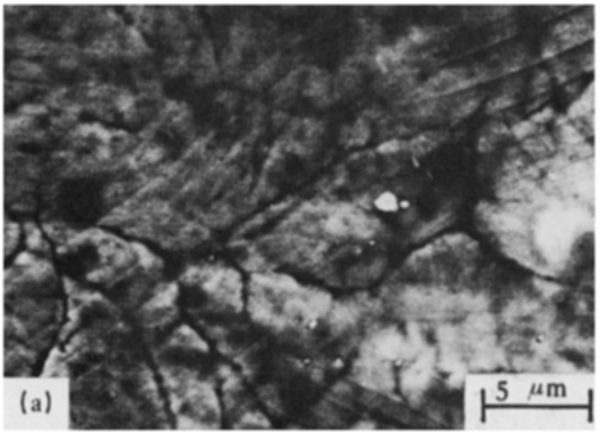

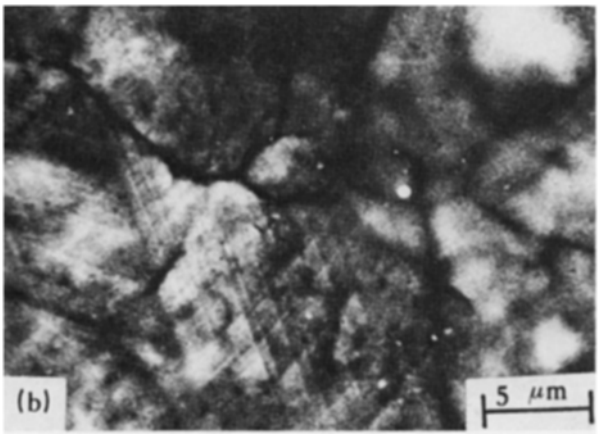

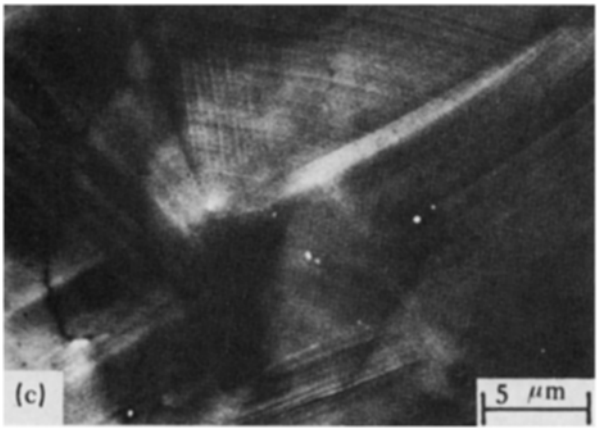

Figure 3 Comparable slip line development for solution-treated specimens tested at different maximum stress amplitudes: (a) 80% of life at $\sigma_{max} = 559$ MPa, (b) 55% of life at $\sigma_{max} = 669$ MPa, and (c) 5% of life at $\sigma_{max} = 779$ MPa.

Finally, the density of cracks which nucleate prior to complete failure is dependent on the magnitude of the maximum stress. Fig. 6 shows the specimen surfaces after failure for solution-treated specimens tested at three different maximum stress levels. At the lowest stress, no fatigue cracks other than that which caused failure appear to have been initiated. At higher maximum stress levels the number of cracks on the surface increases markedly. Fig. 6d exhibits persistent slip bands extending into the bulk along the crack surface. It is evident from Fig. 7 that aged specimens follow the same pattern as the solution-treated specimens.

3.3. X-ray diffraction

Line profile breadths were measured for solution-treated specimens at various fractions of life and are plotted in Fig. 8. The three stress levels employed were 559, 669 and 779 MPa. The data were obtained for the (1 1 1) and (2 0 0) diffraction peaks. A similar dependence of the line breadths on fraction of life was obtained for aged specimens cycled at maximum stress levels of 786 and 979 MPa, as shown in Fig. 9.

A strong dependence of the broadening on the stress level is evident, with higher stress amplitude giving rise to greater broadening. After 10 to 15% of life, the breadths generally decrease slightly and assume a shallow, positive slope thereafter. The degree of broadening is greater for the (2 0 0) crystallographic planes as expected from the functional relationship between the broadening and the Bragg angle, θ. The total broadening is composed of contributions due to microstrain and crystallite size, which are given by

$$\beta_{\text{microstrain}} = -2(\Delta d/d) \tan\theta,$$

and

$$\beta_{\text{crystallite size}} = k\lambda/D \cos\theta$$

where d is the interplanar spacing, θ is the diffraction angle, λ is the X-ray wavelength, k is a constant and D is the crystallite size [28, 29].

The degree of broadening for a *given* $(h\,k\,l)$ is also seen to depend strongly on the maximum stress level. In as much as both the plastic strain associated with the cycling and the density of fatigue cracks increase with the cyclic stress amplitude, it is not surprising that the levels of broadening increase significantly as well. It is important to bear in mind that the line broadening technique averages the deformation accrued by the grains in the fatigued metal. During fatigue, for which the damage is usually localized near stress concentrations or in grains oriented for high resolved shear stress, many grains may undergo only limited or no deformation but will (nevertheless) contribute to the diffraction profile. This volume of material then serves to camouflage the substantial distortions which take place locally during the fatigue life, thus leading to only moderate breadth expansions. The double crystal diffraction arrangement affords a way to circumvent this problem.

Double crystal diffractometry enables the grains at the specimen surface to be individually resolved, so that those incurring distortion can be distinguished from those that are not. The results of the rocking curve analyses for solution-treated specimens are given in Fig. 10. The integrated breadths are plotted as a function of fatigue life fraction for three stress amplitudues: 559, 600 and 669 MPa. The breadths exhibit a tendency for rapid, early-life expansion, followed by some recovery. Thereafter, a steep dependence on the fraction of life is evident up to the time of failure. The differences in the magnitude of the broadening at any particular fraction of life among the three stress levels are a function, primarily, of the intrinsic breadths measured for the virgin specimen.

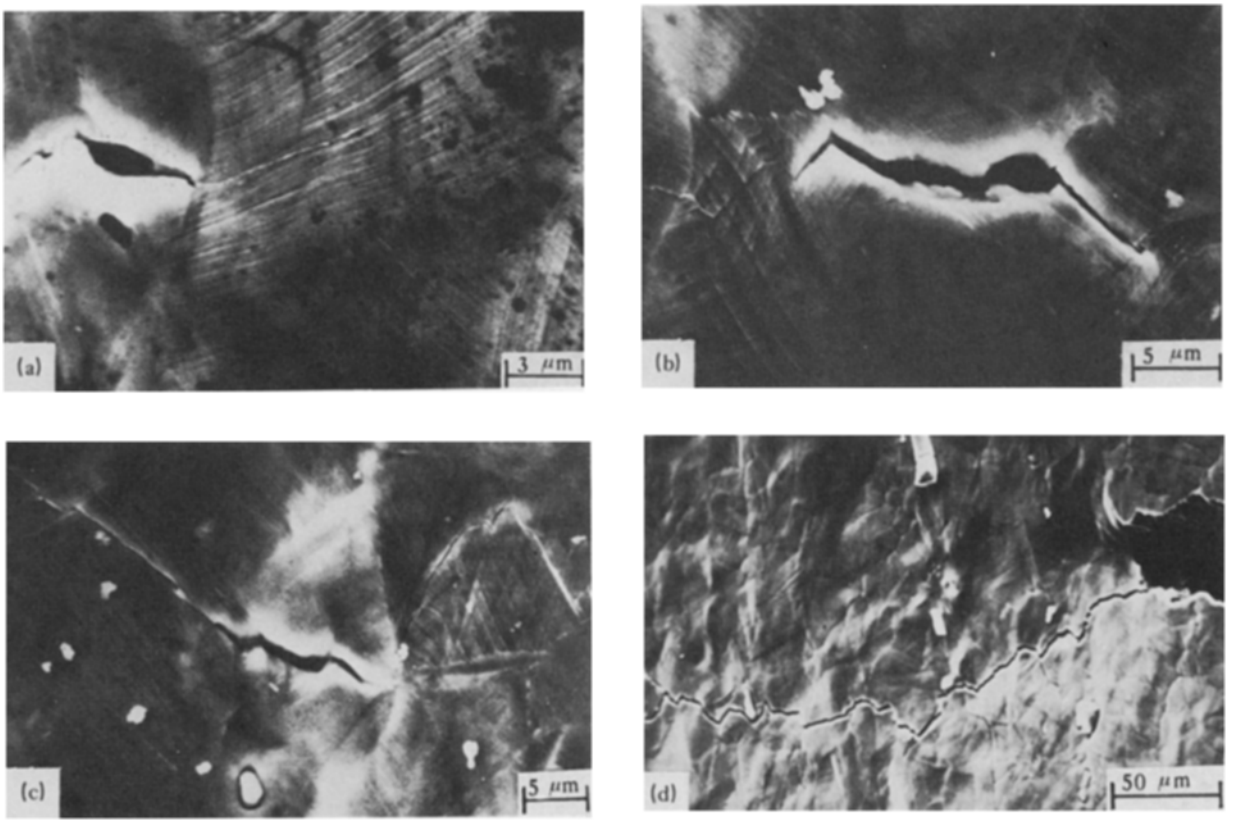

Figure 4 Slip line development and crack initiation and growth during the life for a solution-treated specimen cycled at a maximum stress level of 779 MPa; (a) intense slip lines at 44% of life, (b) multiple slip at tips of propagating crack, (c) and (d) crack growth in direction of slip lines and along grain boundaries.

By normalizing the breadths with respect to the respective virgin specimen breadth, the data fall close to a single line as shown in Fig. 11. Since all the data fall within 15 to 20% of life from the best-fit line, a reasonable estimate of expended life could be made on the basis of the measured rocking curve breadth, regardless of the stress amplitude.

Fig. 12 presents the results of rocking curve breadth measurements as a function of the fatigue life fraction for aged specimens cycled to failure at constant maximum stress amplitudes of 786 and 979 MPa. Again, the broadening of the rocking curves during the life is similar for the two stress levels. Fig. 13 compares the average dependence of the breadths on the fraction of life for the solution-treated material (from Fig. 10) and the aged samples. It can be seen that the aged material gives a line with shallower slope, possibly caused by the reduced tendency for unobstructed slip.

3.4. Spectrum fatigue

Having established the dependence of the line profile and rocking curve breadths on the stress amplitude and fatigue life fraction, an investigation was undertaken to evaluate the effect of changes in the maximum stress *during* the life. Thus far, only solution-treated specimens have been subjected to spectrum fatigue, and only with periodic *decrements* in the maximum stress level. The specimens were fatigued in blocks of cycles estimated at 20 or 25% of life as determined from the *S–N* curve, using a lower maximum

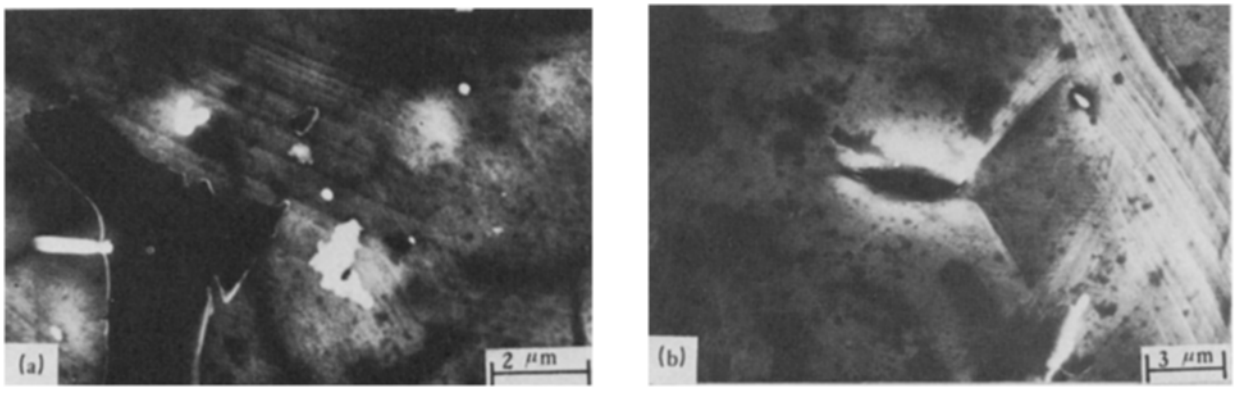

Figure 5 Fatigue cracks in solution-treated specimens tested at low and high maximum stress amplitudes; (a) crack tip region in specimen fatigued at σ_{max} of 669 MPa (N_i = 75% at this stress level) and (b) microcrack in specimen fatigued at 779 MPa (N_i = 20 to 25%). Note slip line formation and then opening of crack along directions consistent with those for slip.

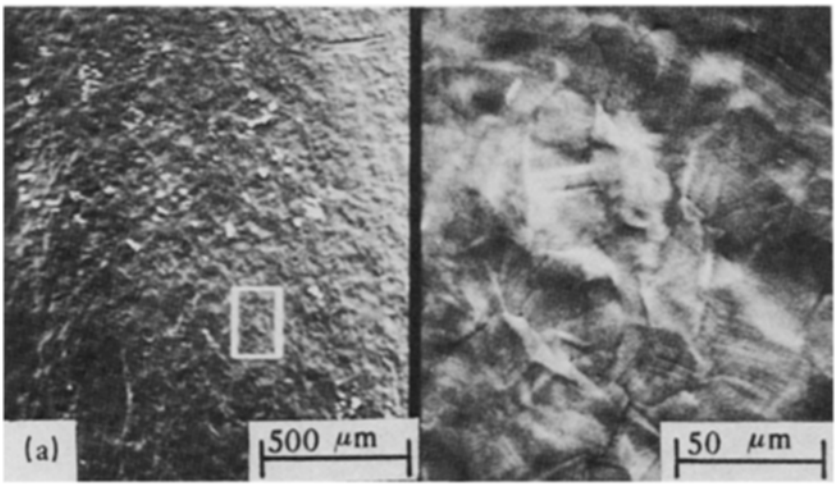

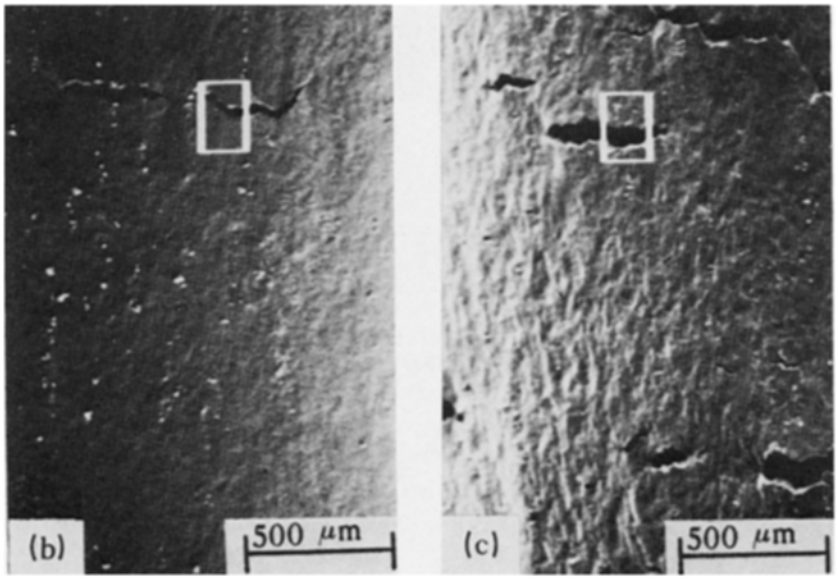

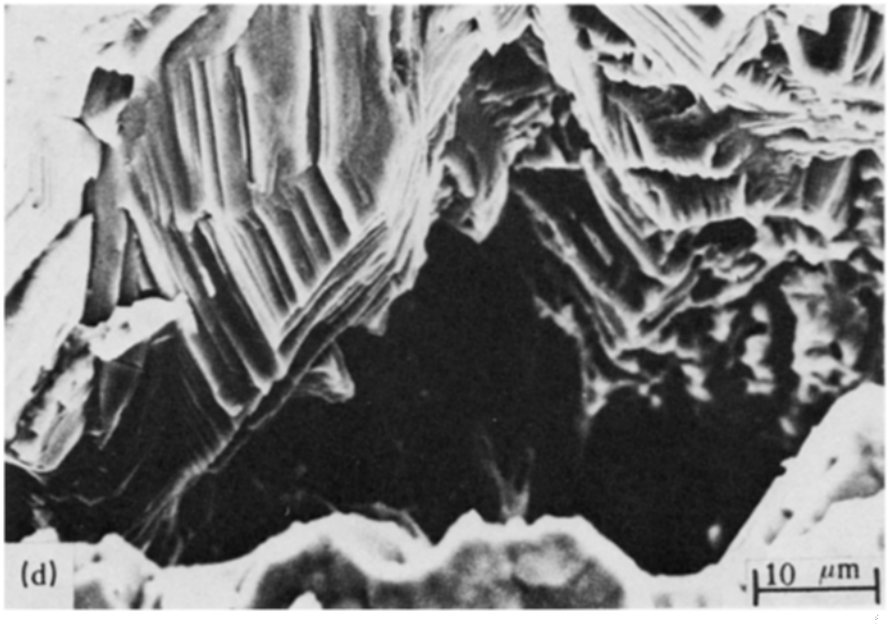

Figure 6 Specimen surfaces after failure for solution treated material fatigued at various maximum stress amplitudes. (a) σ_{max} = 559 MPa, (b) σ_{max} = 669 MPa, (c) σ_{max} = 779 MPa, and (d) persistant slip bands along crack surfaces extending into the specimen interior.

stress for each consecutive block. Line broadening and rocking curve analyses were performed after each block of cycles. Once the specimens had failed, the actual number of cycles to failure was used to adjust the estimated fractions of life after each of the blocks to reflect values consistent with the "true" fatigue life of the sample. Table I summarizes the test conditions and results for the two specimens studied. Fig. 14 shows the rocking curve breadths as a function of the actual fractions of life for the spectrum fatigue specimens (column 3 in Table I). By normalizing these data with respect to the breadths of the virgin

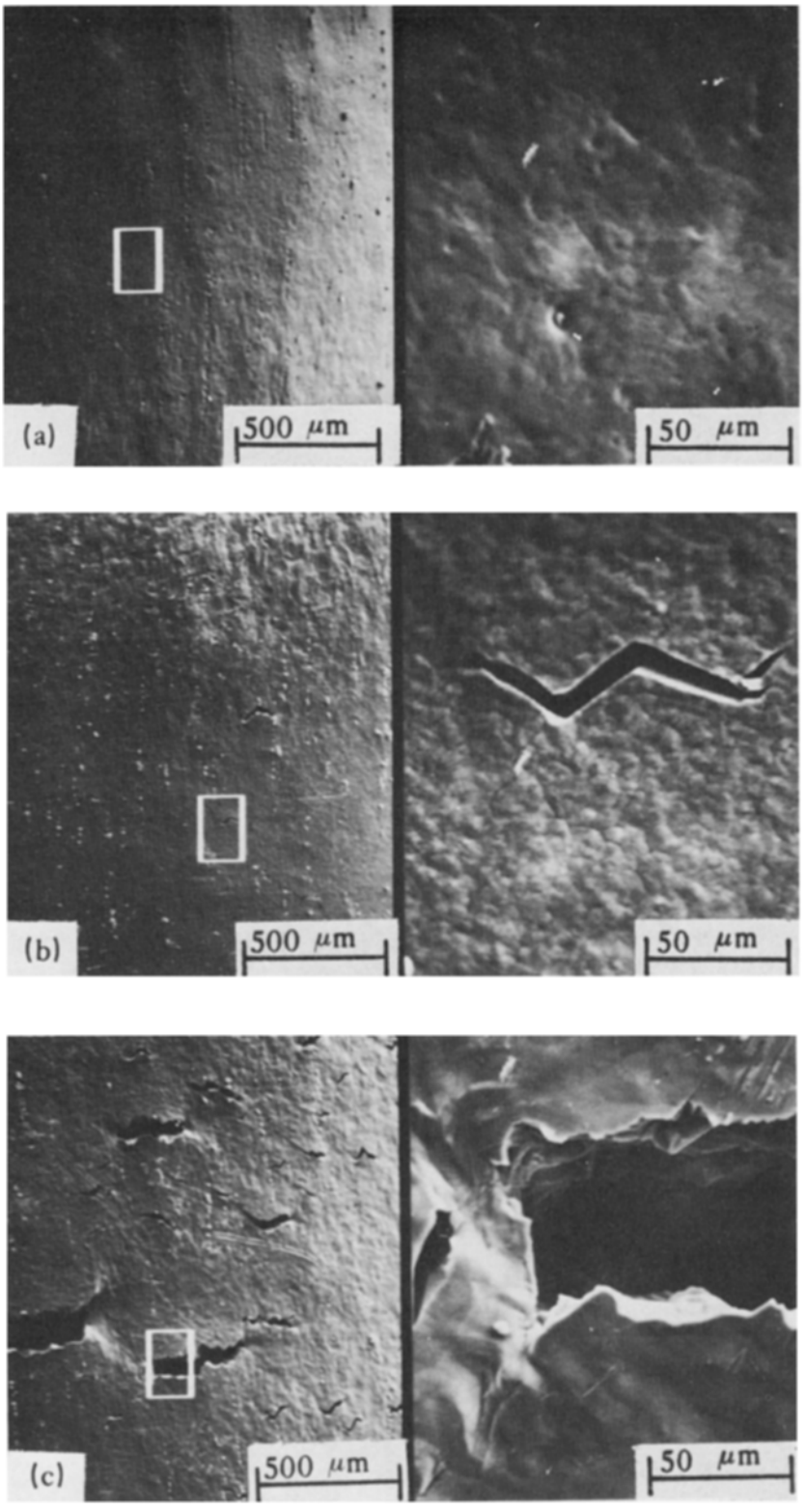

Figure 7 Specimen surfaces after failure for aged material fatigued at various maximum stress amplitudes. (a) $\sigma_{max} = 786$ MPa, (b) $\sigma_{max} = 882$ MPa, (c) $\sigma_{max} = 1076$ MPa.

TABLE I Results of spectrum fatigue tests

	Maximum stress level, σ_{max} (MPa)	Expended life (Miner's linear cumulative damage rule) (%)	Actual expended life (computed from cycles to failure (%)	Estimated expended life (from rocking curve breadth measurements) (%)
Specimen A	669	20	22	22
	641	40	44	45
	614	60	65	62
	586	80	87	79
	559	100	100	
Specimen B	724	25	32	37
	669	50	65	63
	614	75	97	83
	559	100	100	

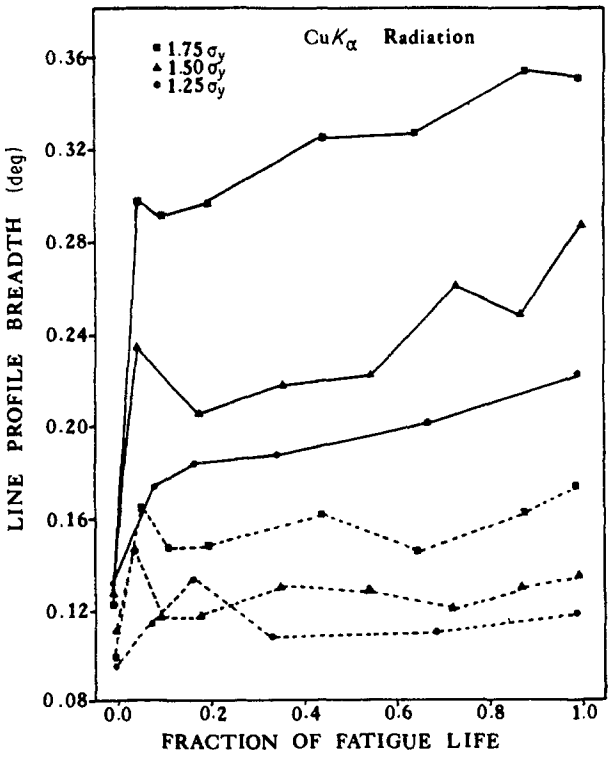

Figure 8 Dependence of line profile breadths on fraction of life for solution-treated specimens tested at three maximum stress levels: 559, 669 and 779 MPa; $R = 0.1$. Solid lines represent (2 0 0) and broken lines represent (1 1 1) set of planes.

specimens and referring to the "calibration" line in Fig. 10, the expended life can be estimated solely on the basis of the measured breadths. These estimates are tabulated in the last column of Table I and exhibit very good agreement with the actual expended life throughout the early and mid-life fractions. Fig. 15 demonstrates this graphically; only at the fractions of life near ultimate failure do the rocking curve breadths deviate significantly from the calibration line. It is important to remember that no knowledge of cyclic history is necessary in order to estimate the expended life in this fashion.

For the second spectrum fatigue test (specimen B), the line profile breadths were also monitored during the life. The results shown in Fig. 16 illustrate that the level of line broadening is consistent with the maximum cyclic stress level employed in the spectrum fatigue sequence. By comparison with the curves in Fig. 8, the measured breadths would suggest a maximum stress level of between 1.5 and 1.75 times the yield strength. The highest maximum stress used in the test was, in fact, $1.625\,\sigma_y$.

3.5. Depth studies

In order to examine the difference between the surface and subsurface response to the fatigue cycling, X-ray rocking curve measurements were made after removing layers of material by electropolishing. Fig. 17 illustrates the results for an aged specimen fatigued at a maximum stress of 883 MPa to 7.5% of life. The depths shown in the graph represent the total thickness of the layers removed and the horizontal line represents the intrinsic breadth for the virgin specimen. At this relatively low fraction of life, it can be seen that the breadths at the surface have undergone considerably greater expansion than those for the interior. A decreasing gradient persists from the surface to a depth of about 40 μm, followed by an increase to a plateau level established at about 75 μm and extending into the bulk. These results are in good agreement with previous findings for Al 2024 [18] fatigued in tension–compression, which showed that the surface distortions occur early in the life as

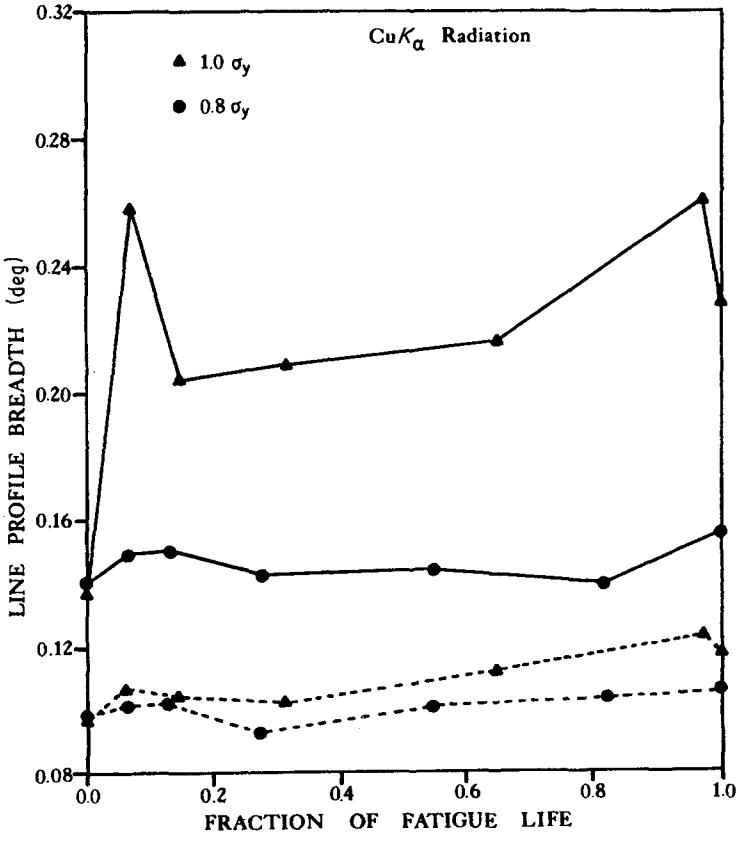

Figure 9 Variation of line profile breadths with fraction of the fatigue life for aged specimens fatigued at maximum stress levels of 786 and 979 MPa. Solid lines represent (2 0 0) and broken lines represent (1 1 1) sets of planes.

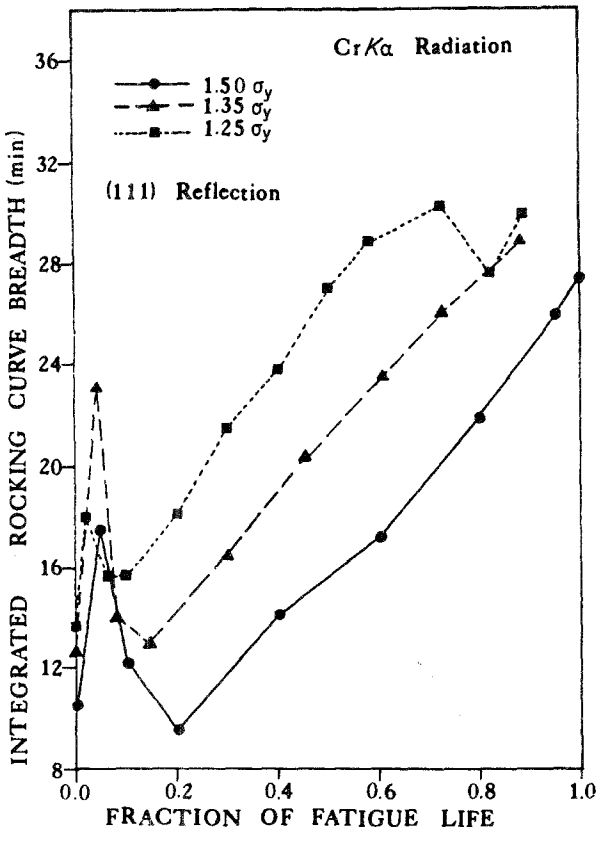

Figure 10 Rocking curve breadths for solution-treated specimens cycled to failure at maximum stress amplitudes of 559, 600 and 669 MPa.

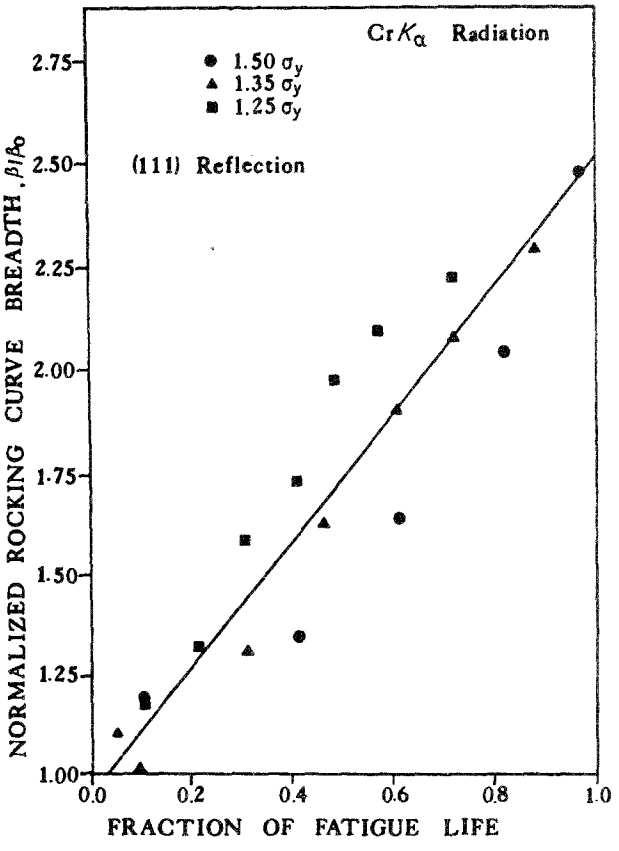

Figure 11 Normalized rocking curve breadths from Fig. 9 as a function of the fraction of the fatigue life (β_0 is the intrinsic breadth for the virgin specimen).

compared to a more gradual change in the subsurface material.

4. Conclusions

1. The fatigue behaviour of Inconel 718 has been characterized for the solutionized and aged conditions through *S–N* diagrams, measurements of cumulative lattice distortion during the life, and observations of slip band development and crack initiation and growth.

2. The number of cycles to failure is larger for aged samples as compared to solutionized specimens for all

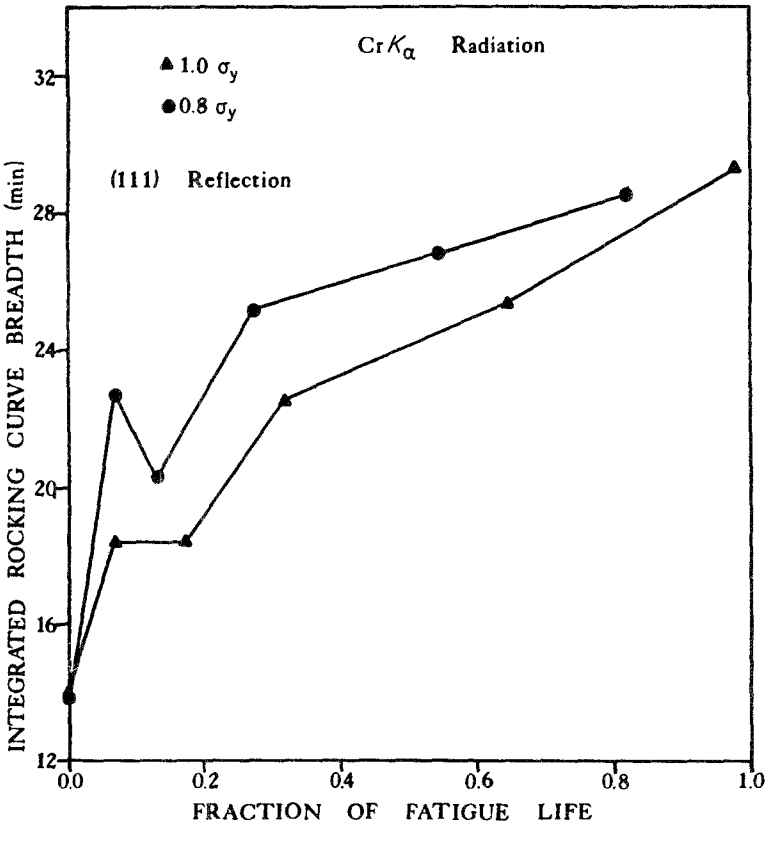

Figure 12 Rocking curve breadths for aged specimens cycled to failure at two different maximum stress amplitudes: 786 and 979 MPa.

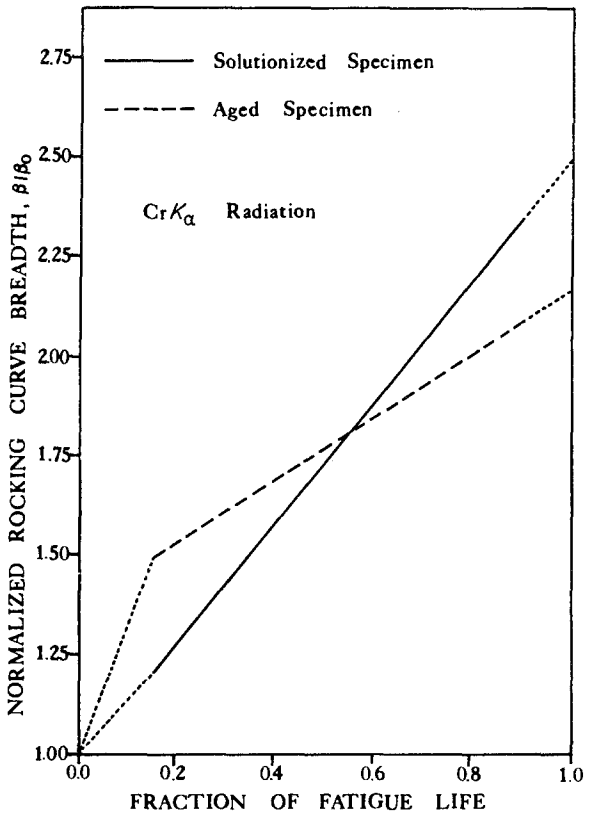

Figure 13 Comparison of "calibration" curves for solutionized specimens and aged specimens showing the relative dependence of the rocking curve breadths on fraction of life.

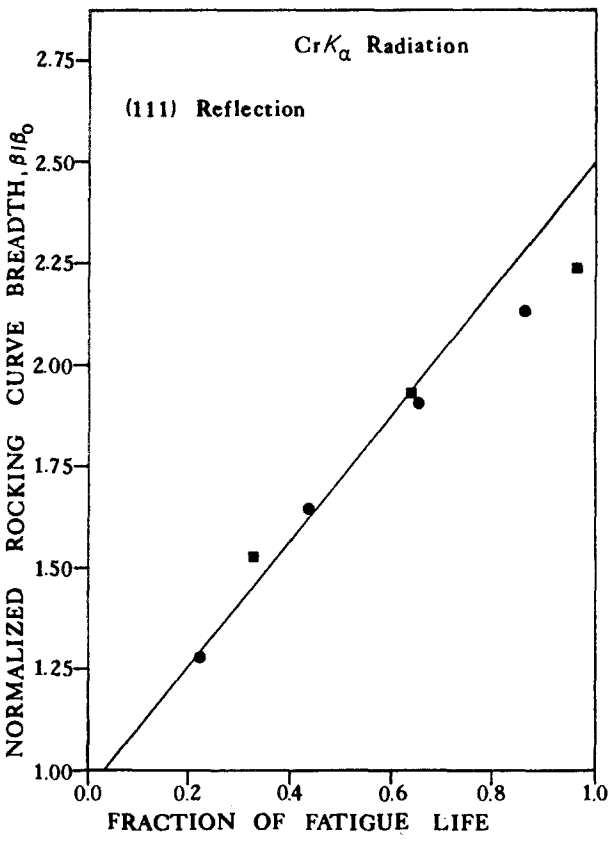

Figure 15 Normalized rocking curve breadths for spectrum fatigue specimens A and B. Solid line is in the "calibration" curve for solution treated material from Fig. 10.

stress levels examined. Over the range of lifetimes investigated, the maximum stress levels represent smaller fractions of the respective yield strength for the aged material than do those for the solution-treated material.

3. Two X-ray diffraction methods were found useful in evaluating the microstructural changes associated with cyclic deformation. X-ray line broadening is sensitive to the magnitude of the maximum stress level employed in the fatigue testing and provides a

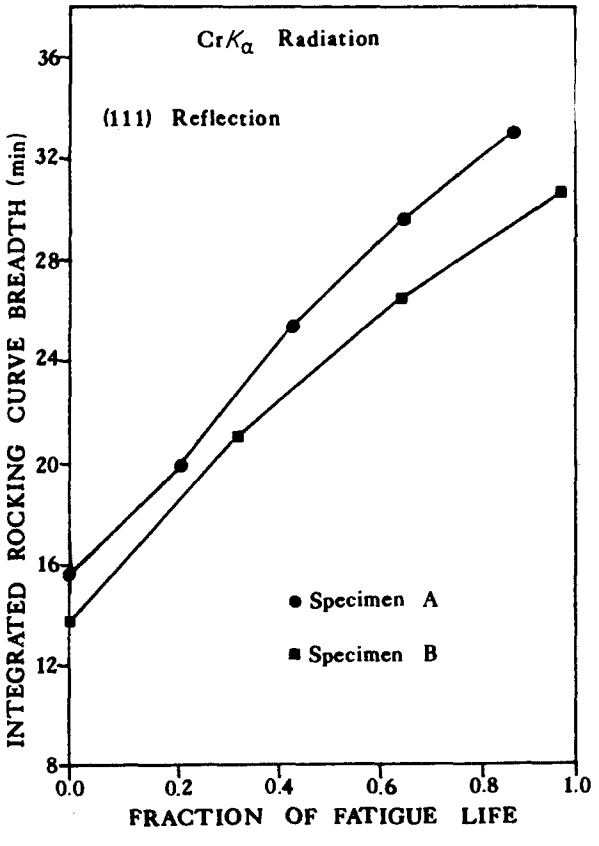

Figure 14 Rocking curve breadths for two spectrum fatigue specimens as a function of actual fatigue life fraction.

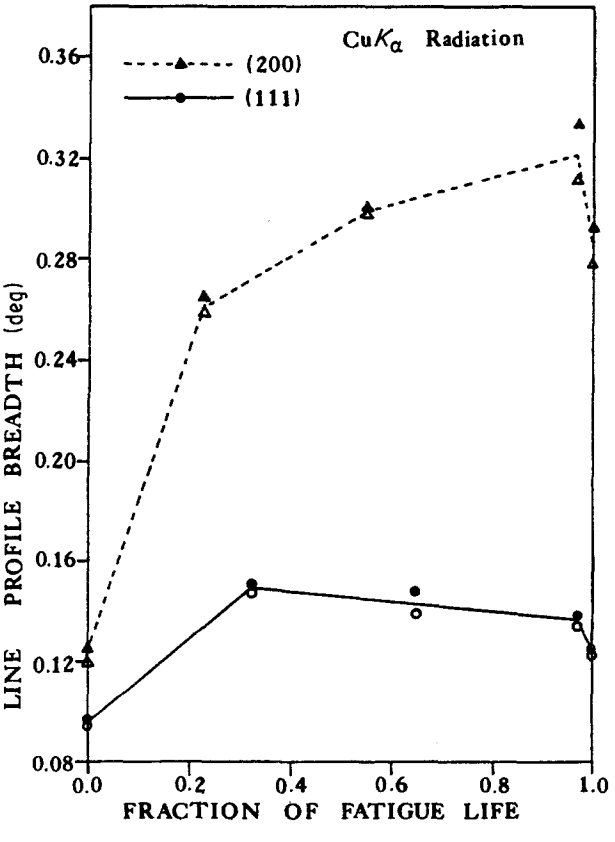

Figure 16 Variation of the line profile breadths with fraction of fatigue life for spectrum fatigue specimen B.

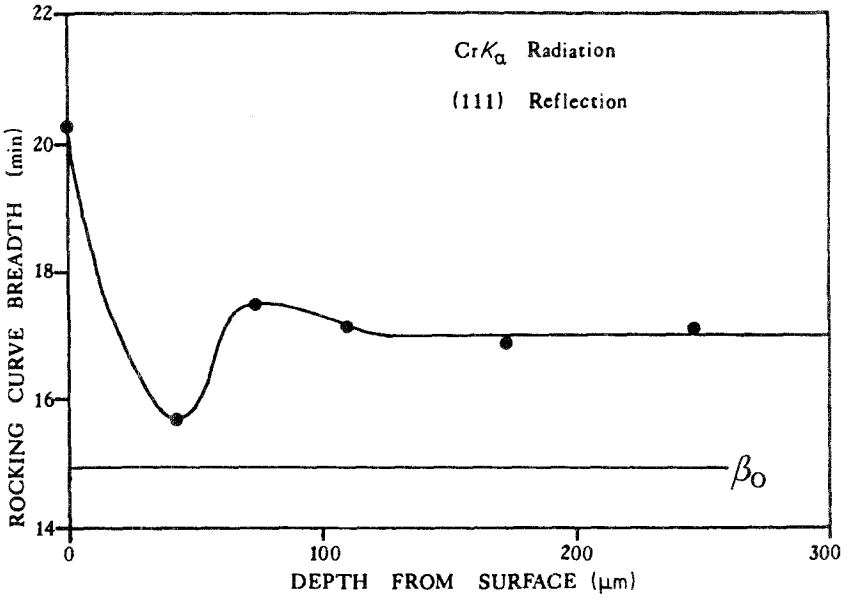

Figure 17 Depth profile for an aged specimen fatigued at 883 MPa maximum stress to 7.5% of life. Depths correspond to the layer thickness removed from the surface by electropolishing. (β_0 is the intrinsic breadth for the virgin specimen).

measure of the average plasticity inherent to the test conditions. X-ray rocking curve breadths show much greater sensitivity to the accumulation of lattice distortion during the life, irrespective of the cyclic stress level.

4. The rate of slip band development, fraction of life at which cracks are initiated and density of cracks visible on the surface are all dependent on the maximum stress amplitude of the test. The severity of the slip line formation is less for the aged material as is the degree of X-ray rocking curve broadening which occurs during the life. Depth profiles obtained by double crystal diffractometry also indicate that the induced lattice distortions are greater at the surface than in the bulk, at least during the early fractions of life.

5. The combination of X-ray diffraction techniques has proved to be useful for estimating the expended fraction of life and highest cyclic stress level to which a spectrum fatigued sample has been subjected, even in the absence of any knowledge of prior cyclic history.

Acknowledgement

The authors wish to thank the General Electric Company for its generous support of these investigations.

References

1. M. CLAVEL and A. PINEAU, *Met. Trans.* **9A** (1978) 471.
2. T. H. SANDERS JR, R. E. FRISHMUTH and G. T. EMBLEY, *ibid.* **12A** (1981) 1003.
3. P. SHAHINIAN and K. SADANANDA, in "Proceedings of International Conference on Engineering Aspect of Creep", Vol. 2 (Society of Automotive Engineers, 1980) p. 1.
4. S. D. ANTOLOVICH and N. JAYRAMAN, in "Proceedings of Sagamore Army Materials Research Conference, Vol. 27 (Plenum Press, New York, 1980) p. 119.
5. D. FOURNIER and A. PINEAU, *Met. Trans.* **8A** (1977) 1095.
6. H. F. MERRICK, *ibid.* **5** (1974) 891.
7. I. KIRMAN and D. H. WARRINGTON, *ibid.* **1** (1970) 2667.
8. J. L. FIELD, F. BEHNAZ and R. N. PANGBORN, ASTM-STP 811 (American Society for Testing and Materials, Philadelphia, 1983) p. 71.
9. V. WEISS, Y. OSHIDA and A. WU, *Fatigue Eng. Mater. Struc.* **1** (1979) 333.
10. S. TAIRA and K. HAYASHI, in "Proceedings of the 9th Japanese Congress on Testing of Materials" (Society of Materials Science, Kyoto, 1966) p. 1.
11. V. V. KORCHEVSKIY and L. P. METLITSKAYA, *Phys. Met. Metall.* **50** (1980) 152.
12. H. TAKECHI, K. NAMBA, K. FUJIWARA and K. KAWASAKI, *Trans. Iron Steel Inst. Jpn.* **21** (1981) 92.
13. S. TAIRA, T. GOTO and Y. NAKANO, in "Proceedings of 12th Japanese Conference on Materials Research" (Society of Materials Science, Kyoto, 1969) p. 8.
14. B. PATHIRAJ and R. VASUDEVAN, in "Proceedings of Fracture Mechanics and Technology" (Hong Kong, 1977) p. 1593.
15. S. TAIRA and K. KAMACHI, in "Proceedings of Sagamore Army Materials Research Conference, Vol. 23 (Plenum Press, New York, 1976) p. 21.
16. V. WEISS, Y. OSHIDA and A. WU, *J. Nondest. Eval.* **1** (3) (1980) 207.
17. I. R. KRAMER, R. N. PANGBORN and S. WEISSMANN, in "Proceedings of Sagamore Army Material Research Conference", Vol. 27 (Plenum Press, New York, 1980) p. 103.
18. R. N. PANGBORN, S. WEISSMANN and I. R. KRAMER, *Met. Trans.* **12A** (1981) 109.
19. *Idem, Adv. X-ray Anal.* **24** (1981) 203.
20. R. N. PANGBORN, R. YAZICI, T. TSAKALAKOS, S. WEISSMANN and I. R. KRAMER, in "Proceedings of Symposium on Accuracy in Powder Diffraction", (National Bureau of Standards Special Publication 567, Gaithersbury, 1979) p. 443.
21. R. YAZICI, W. MAYO, T. TAKEMOTO and S. WEISSMANN, *J. Appl. Cryst.* **16** (1983) 1.
22. S. WEISSMANN, Report from MRL to Bureau of Engineering Research, Rutgers University (1956).
23. 1984 Annual Book of ASTM, B637-84 (1984) p. 722.
24. W. A. RACHINGER, *J. Sci. Instrum.* **25** (1948) 254.
25. T. S. COOK, G. E. Aircraft Engine Group, unpublished results (1984).
26. J. K. TIEN and R. P. GAMBLE, *Met. Trans.* **2** (1971) 1933.
27. M. GELL and G. R. LEVERANT, *Trans. AIME* **242** (1968) 1869.
28. A. R. STOKES and J. C. WILSON, *Proc. Phys. Soc. Lond.* **56** (1944) 174.
29. F. SCHERRER, *Gottingen Nachrichten* **2** (1918) 98.

Received 28 February
and accepted 20 March 1985